CrossMark

Critical stiffness damage envelopes for multidirectional laminated structures under multiaxial loading conditions

John Montesano, Chandra Veer Singh *

Materials Science and Eng., University of Toronto, 184 College St., Suite 140, Toronto M5S 3E4, Canada

ABSTRACT

Load-bearing laminated structures undergo complex crack evolution processes and consequent stiffness degradation, which leads to a decline in their overall performance. Thus, consideration of damage evolution is important for stiffness critical applications. In this study, a multi-scale damage model combining synergistic damage mechanics (SDM) with an energy-based damage evolution model is developed for multidirectional laminated structures. The SDM approach combines computational finite element-based micromechanics with continuum damage mechanics, enabling the evaluation of the laminate stiffness. The damage model predicts evolution of sub-critical matrix cracks in different plies under multiaxial loading. Model predictions, which include ply crack density evolution and laminate stiffness degradation, correlate well with available experimental data, while model results for various CFRP and GFRP multidirectional laminates demonstrate its robustness. Additionally, damage envelopes corresponding to pre-selected critical stiffness degradation levels are developed to serve as an alternative to current approaches of final failure envelopes, and are regarded as a useful design tool for stiffness critical composite structures in practical applications.

© 2015 Published by Elsevier Ltd.

1. Introduction

For practical load bearing composite structures, laminates with multidirectional plies are often utilized to provide comprehensive directional strength and stiffness properties. The nature of the damage evolution in these laminates under realistic multiaxial loading conditions involves the progression of ply cracks in multiple orientations. These ply cracks, which span the ply thickness and are oriented along the fiber direction in respective plies, begin to interact and influence the ply constraining effects (see Fig. 1), whereby a complex three-dimensional stress state ensues. Being subcritical in nature, this damage, even at high crack densities, does not typically lead to catastrophic structural failure, although they may cause onset of critical damage modes such as delamination and fiber fracture [1]. Nevertheless, ply cracking does cause a progressive degradation of the laminate stiffness due to stress redistribution near cracks. This may lead to a decline in the overall performance, such as a loss in structural rigidity and increased deformation under service loads. In addition, since the dynamic stiffness of the structure will be greatly diminished, its natural frequencies will continually reduce as ply cracks progressively evolve [2]. Thus, a thorough understanding of the progressive nature of this failure process in multidirectional composites is important, especially for stiffness critical applications.

The common industry practice is to use failure theories such as the well-known Tsai–Wu criteria or Puck's criteria for the design of composite structures. An assessment of these failure theories has recently been reported in Ref. [3]. The main limitations with failure theories for composite structures in general are (*i*) they do not properly account for physical damage mechanisms, and (*ii*) they cannot adequately account for the in-situ ply constraining effects in laminates. The inability of various progressive failure models that incorporate these failure theories to accurately predict final failure envelopes for a number of defined test cases was illustrated through the recent world-wide failure exercise (WWFE) [4]. A more suitable approach is to directly consider the progressive failure process, whereby crack evolution and its influence on the laminate stiffness are explicitly accounted for, which is accomplished by damage mechanics based progressive failure models. In this respect, critical stiffness criteria can be proposed as an alternate to traditional failure criteria. For many practical composite structures, such as automotive, aircraft and wind turbine structures, stiffness based criteria is more useful.

The problem of subcritical damage evolution in laminated composites has been investigated extensively [5–8]; however most of the reported studies consider uniaxially loaded cross-ply laminates containing cracks in only the 90° plies. Ply crack evolution in multidirectional laminates has also been investigated, but mainly under uniaxial loading conditions [9–12]. On the other hand, many of the existing models that consider multi-axial loading [13–23] are not applicable to multidirectional laminates involving ply cracking in multiple orientations. This is partly due to the fact that some of them provide closed-

* Corresponding author.
E-mail addresses: john.montesano@utoronto.ca (J. Montesano), chandrveer.singh@utoronto.ca (C.V. Singh).
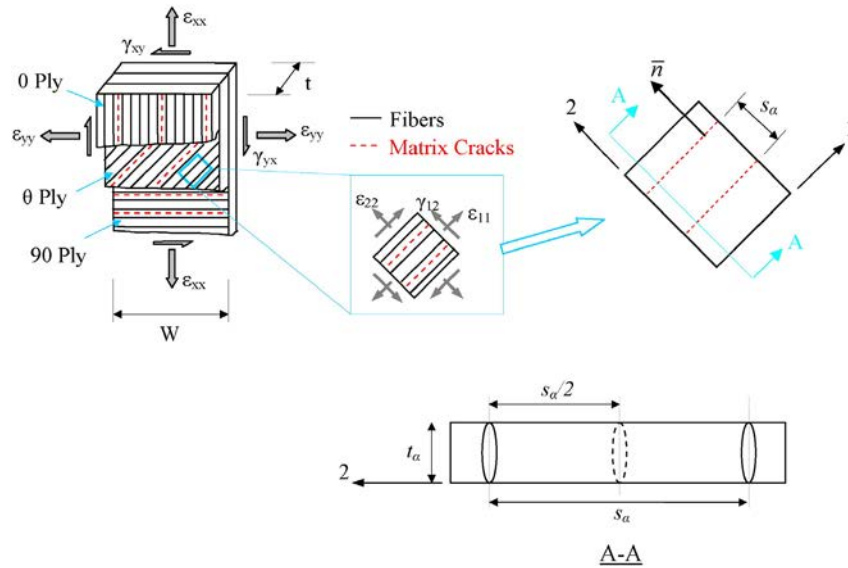
Fig. 1. A representative volume element of a damaged multidirectional laminate subjected to an in-plane multiaxial strain state. The local transformed strain components and the crack spacing are also shown.

form solutions only applicable for cross-ply laminates. Other models utilize ultimate failure criteria to predict traditional failure envelopes, without considering the actual progression of damage. Some models also utilize finite element analysis to simulate damage progression in multidirectional laminates as was described in the review by Liu and Zheng [17], but they fail to account for the evolution of actual damage modes and do not accurately predict the corresponding stiffness degradation. Also, the practical application of many models is limited as they rely on extensive empirical data for calibration. In general, existing models fail to combine damage evolution with stiffness degradation in a coherent fashion, which renders them inadequate for the analysis of practical stiffness critical structures.

Montesano and Singh [24,25] have recently addressed some of these modeling limitations through a multiscale progressive synergistic damage mechanics (SDM) model, wherein damage evolution in cross-ply laminates subjected to multiaxial loading was predicted using an energy approach. The model combines computational micromechanics with continuum damage mechanics (CDM) for evaluating the corresponding laminate stiffness degradation. The main goal of this study is to extend this comprehensive model to the case of multidirectional composite laminates subjected to multiaxial loading, which is not a trivial task. Additional modeling considerations such as evaluation of the ply-dependent critical crack energy release rates must be accounted for, which will be discussed. To the knowledge of the authors, this is the only model reported that can predict damage evolution in multiple plies of different orientations simultaneously, as well as the corresponding stiffness degradation, of multidirectional laminates under multiaxial loading conditions. Furthermore, we also introduce the concept of critical stiffness damage envelopes which are generated for many multidirectional laminates. Their utility as robust and more practical design criteria for stiffness critical structures is discussed.

2. Analytical model

The multi-scale damage prediction model is developed by combining the synergistic damage mechanics (SDM) approach with an energy based damage evolution model. The SDM model enables evaluation of the in-plane stiffness moduli for multidirectional laminates undergoing multi-mode ply cracking under multiaxial loading situations, and will be described first. An energy-based approach to predict the evolution of ply cracks in different off-axis plies under biaxial loading will be subsequently presented.

2.1. Constitutive equations for cracked laminates

The representative volume element (RVE) for a general multidirectional laminate consisting of cracked on-axis, off-axis and transverse plies, and subjected to a general in-plane multiaxial applied strain state is shown in Fig. 1. Assuming that the ply cracks in a given ply of arbitrary orientation are uniformly spaced, self-similar and fully developed through the lamina thickness and RVE width, then following the typical CDM approach, the damage state within the laminate volume, corresponding to a particular damage mode α, can be described through a second-order damage tensor as [26]:

$$D_{ij}^{(\alpha)} = \frac{\kappa_\alpha t_\alpha^2}{s_\alpha t} n_i n_j = D_\alpha n_i n_j. \tag{1}$$

Here, t_α is the cracked ply thickness, s_α is the average crack spacing, n_i are components of the crack surface normal unit vector (see Fig. 1), and κ_α is a constraint parameter that represents the corresponding ply constraining effect, which is a function of the crack opening displacement (COD). Considering thin symmetric orthotropic laminates, the Helmholtz free energy for the damaged laminate is formulated in terms of applied strain and damage tensor components, $\psi(\varepsilon_{ij}, D_{ij}^{(\alpha)})$. Following the Clausius–Duhem inequality and relating ψ to the resultant stress tensor, σ_{ij}, the overall stress–strain relationships for the damaged laminate are derived as:

$$\sigma_{ij} = C_{ijkl}\left(D_{ij}^{(\alpha)}(\rho)\right)\varepsilon_{kl} \tag{2}$$

where stiffness properties at given crack density ρ are defined by [24]:

$$C_{ijkl} = \begin{bmatrix} \dfrac{E_x^o}{1-\nu_{xy}^o\nu_{yx}^o} & \dfrac{\nu_{xy}^o E_y^o}{1-\nu_{xy}^o\nu_{yx}^o} & 0 \\[3mm] \dfrac{\nu_{xy}^o E_y^o}{1-\nu_{xy}^o\nu_{yx}^o} & \dfrac{E_y^o}{1-\nu_{xy}^o\nu_{yx}^o} & 0 \\[3mm] 0 & 0 & G_{xy}^o \end{bmatrix} - \sum_\alpha a_\alpha D_\alpha \begin{bmatrix} 2a_1^{(\alpha)} & a_4^{(\alpha)} & 0 \\ a_4^{(\alpha)} & 2a_2^{(\alpha)} & 0 \\ 0 & 0 & 2a_3^{(\alpha)} \end{bmatrix}. \tag{3}$$

The first term on the right hand side of Eq. (3) represents the stiffness matrix for the undamaged laminate evaluated using classical laminate theory (CLT), whereas the second term represents the stiffness changes brought about by damage in different modes. Here, the $a_i^{(\alpha)}$ terms are a set of phenomenological laminate damage constants corresponding to a

specific damage mode α, and the D_α terms are the effective damage parameters represented in Eq. (1).

The expression in Eq. (3) can be used to evaluate the total stiffness tensor for any general symmetric laminate subjected to in-plane multi-axial loading, and containing any number of damage modes, so long as the constraint parameters (κ_α) and the damage constants ($a_i^{(\alpha)}$) for all damage modes can be evaluated. In lieu of costly experimental data, the κ_α and $a_i^{(\alpha)}$ terms are evaluated here by using 3D micromechanical FE models. The details of the computational micromechanical models are provided in Ref. [24], thus only the main points will be discussed here for brevity. Three-dimensional models were used in order to accurately capture the effects of ply constraining on the ply crack surface displacements, as well as inter-ply and intra-ply crack interactions. The RVE of the laminate was represented in the computational model using transversely orthotropic elastic plies of suitable thickness, and meshed with 3D continuum elements using the commercial FE software ANSYS. Cracks spanning the ply thickness were explicitly included in the FE models as discontinuities between elements, where scenarios with cracks in multiple plies were considered. Periodic boundary conditions were then applied to the meshed laminate RVE, which allowed for proper representation of the laminate shear response under multiaxial loading. In order to computationally evaluate the constraint parameters for a specific damage state, the corresponding averaged COD was used. Thus, κ_α is defined by:

$$\kappa_\alpha = \frac{(\overline{\Delta u_2})_\alpha}{\varepsilon_{eff} t_\alpha} \tag{4}$$

where $(\overline{\Delta u_2})_\alpha$ is the computationally evaluated averaged COD and is defined as the normal separation between crack faces (i.e., direction 2 in Fig. 1), and ε_{eff} is the effective strain contributing to the COD in a multiaxial loading condition. Finally, a scheme was devised where volume averaged strains and stresses extracted from the computational micromechanical models were used along with Eq. (3) in order to evaluate the $a_i^{(\alpha)}$ constants [24] for a specific laminate.

2.2. Energy model for damage evolution

An energy approach based on the concepts of linear elastic fracture mechanics has been developed to predict the evolution of subcritical ply cracks in multidirectional laminates subjected to multiaxial loading conditions. Consider two cracks states for an arbitrarily oriented ply in a laminate with crack spacing denoted by s_α and $s_\alpha/2$ as shown in Fig. 1. Upon increasing the applied load additional cracks may form, increasing the number of cracks from N to $2N$. It should be noted that it is assumed the ply crack spacing will remain uniform as new cracks multiply. If the energy associated with mode I is considered, the work required to close the new N cracks is defined by [11,25]:

$$W_I = \frac{(\sigma_2^\alpha)^2 t_\alpha}{E_2} \left[2\tilde{u}_n^\alpha(s_\alpha/2) - \tilde{u}_n^\alpha(s_\alpha) \right]. \tag{5}$$

Here, E_2 is the transverse modulus of the undamaged ply, σ_2^α is the transformed far-field ply level stress acting normal to the crack plane evaluated using CLT, and $\tilde{u}_n^\alpha$ denote the normalized average CODs associated with a specific damage mode. In order to capture the crack-shielding effect caused by the interaction of stress fields between adjacent ply cracks, $\tilde{u}_n^\alpha$ are represented by an inverse sigmoidal function of the crack density. These functions are evaluated by varying the crack spacing in the micromechanical FE models for the laminates studied [24]. It should be noted that the energy associated with mode II cracking (i.e., sliding mode) is not considered in this study, and it is not believed to be critical for ply crack multiplication processes. Experimental data reported in Ref. [9] on off-axis cracking in uniaxial tensile loaded $[0/\pm\theta_4/0_{1/2}]_s$ laminates show that for low angles, θ, cracks do not

initiate until final failure, and for larger angles cracks did not form until large axial strains were applied. This suggests that unless the ply tensile stress normal to the crack surface is large enough multiple cracks do not form, and that the shear stress in the ply alone does not form off-axis cracks [11]. Thus, it is reasonable to deduce that the energy associated with shearing is not sufficient to cause ply cracks to initiate.

For any given loading condition, the criterion for crack multiplication in an arbitrarily oriented ply is defined as:

$$\frac{W_I}{G_{Ic}} \geq 1 \tag{6}$$

where, G_{Ic} is the critical strain energy release rate associated with crack multiplication in mode I for a particular ply. Since, the process of crack multiplication in constrained plies is quite different than individual crack extension, G_{Ic} needs to be calibrated. In order to avoid costly experimental testing, we have developed a modified numerical approach based on the well-known crack tip closure technique. This involves a 3D micromechanical FE analysis of the laminate with a fully developed through-the-thickness crack in one given ply as it is constrained by the adjoining uncracked plies. The evaluated COD corresponding to a very large crack spacing (i.e., $s_\alpha = 100 t_\alpha$) is ultimately used to define G_{Ic} as it pertains to the crack initiation process, and this is repeated for each ply in the laminate. The benefit of this economical numerical approach is that distinct G_{Ic} values for crack multiplication in each ply of a laminate of any given stacking sequence can be evaluated. This variation of G_{Ic} for different plies is consistent with findings of Camanho et al. [27], and is a significant contribution to the model development as it is a requirement for accurately predicting damage evolution in multiple plies of a laminate subjected to multiaxial loading.

Furthermore, the prediction model also accounts for the stochastic nature of the ply crack multiplication process, which results from a random distribution of manufacturing flaws, local fiber fractions, or weakened fiber matrix interfaces [28]. A two-parameter Weibull distribution for G_{Ic} is defined as:

$$G_{Ic} = G_o \left[\ln \left(\frac{1}{1-F} \right) \right]^{\frac{1}{m}} \tag{7}$$

where G_o and m are Weibull distribution parameters, and F is a random number in interval [0,1].

The complete procedure for predicting micro-crack initiation and propagation in multiple plies for a general symmetric laminate has been coded into a MATLAB algorithm. The multiaxial quasi-static load applied to the laminate is incremental strain- or stress-controlled loading. The algorithm requires as input the ply engineering constants E_1, E_2, G_{12}, and ν_{12}, the undamaged laminate engineering constants $E_x^o, E_y^o, G_{xy}^o,$ and ν_{xy}^o, the computationally evaluated normalized CODs and $a_i^{(\alpha)}$ damage constants, the ply level G_{Ic} values, and the corresponding Weibull parameters. The main algorithm loop controls the applied loading increments, whereby iterations are performed to determine whether ply crack densities evolve in each ply using the criterion in Eq. (6) at the current applied load level. This process is repeated for all plies in a laminate at every applied load level until the criterion holds true, after which the laminate stiffness tensor, $C_{ijkl}(D_{ij}^{(\alpha)}(\rho))$, is evaluated using Eq. (3). This is repeated for all applied loading levels until a specified stop criterion is met, which is when a critical strain level or a critical stiffness value is attained [25]. This methodology is able to predict the simultaneous evolution of ply cracks in multiple damage modes, while also accounting for crack interactions between adjacent cracked plies though the normalized COD functions.

Table 1
Lamina elastic properties.

Lamina	E_1 (GPa)	E_2 (GPa)	G_{12} (GPa)	ν_{12}	t_{ply} (mm)
T300/934 [7] (for [0/90]$_s$ and [0/90$_2$]$_s$ CFRP laminates)	144.8	11.38	6.48	0.30	0.132
Fiberite/HyE 9082 Af [9] (for [0/+θ_4/−θ_4/0$_{1/2}$]$_s$ GFRP laminates)	44.7	12.7	5.8	0.297	0.125
Silenka E-glass 1200tex/epoxy [30,31] (for [±θ]$_s$ GFRP laminates)	45.6	16.2	5.83	0.278	0.25
E-glass/Epikote [29] (for [0/90]$_s$ and [0/90/∓θ]$_s$ GFRP laminates)	46	13	5	0.30	0.50

3. Results and discussion

The developed model is used to predict the evolution of ply cracks in laminates subjected to multiaxial loading. Thereafter, damage envelopes corresponding to critical stiffness levels are predicted. The proposed critical stiffness damage envelopes can serve as an alternative to traditional failure envelopes, and are regarded by the authors as suitable design criteria for stiffness critical composite structures. To showcase the wide utility of the developed method, a variety of laminates were considered: [0/90]$_s$ and [0/90$_2$]$_s$ cross-ply CFRP [7], [0/90]$_s$ cross-ply and [0/90/∓θ]$_s$ GFRP [29], [0/+θ_4/−θ_4/0$_{1/2}$]$_s$ GFRP [9], and [±θ]$_s$ angle-ply GFRP [30,31]. The elastic moduli and ply thickness for each laminate are detailed in Table 1. Notably, the experimental data for most laminates is typically limited to uniaxial loading conditions, therefore the prediction model is first validated using uniaxial test data reported in the literature. Reported biaxial test data for an angle-ply laminate [30] is also considered for validation.

3.1. Model validation

Computational micromechanics was first utilized to evaluate the normalized CODs, $\tilde{u}_n^\alpha$, and to calibrate damage constants, $a_i^{(\alpha)}$, as required in Eqs. (3)–(5). Furthermore, as indicated before, the ply cracking critical strain energy release rates, G_{Ic}, associated with the crack multiplication of different plies in each laminate are also evaluated using computational micromechanics. Subsequently, using the damage evolution criterion in Eq. (6), predictions for crack density vs. applied loading are made. Fig. 2a shows predictions for 90° ply crack density evolution for two uniaxially loaded cross-ply CFRP laminates, along with corresponding experimental data from Ref. [7]. A clear agreement between model predictions and experimental data can be seen. The model is also able to predict a lower crack initiation stress for the laminate with the thicker 90° ply as reported in previous experimental studies [8]. The constitutive relationship for a damage laminate, Eqs. (2)–(3), allows us to predict normalized shear modulus, G_{xy}/G_{xyo}, for the

[0/90$_2$]$_s$ CFRP laminate, as shown in Fig. 2b, along with available experimental data from Tsai and Daniel [32]. The model results again correlate well with the experimental data, with current model providing more accuracy in comparison to the equivalent constraint model developed by Fan and Zhang [33]. This is very important because it demonstrates that the model captures the shear deformation response accurately for this laminate.

Next, we present predicted crack density plots for a [0/90/∓45]$_s$ quasi-isotropic GFRP laminate with cracks in 90, 45, and −45 plies. As shown in Fig 3a, the results for 90° ply cracking agree well with the experimental data, while the −45° and +45° ply crack initiation strains are consistent with those previously reported in Ref. [29]. It should be noted that the crack densities in the −45° and +45° plies differs due to the fact that then effective thickness of the +45° ply is twice that of the −45° since it is located at the center of the laminate. The stress–strain response, evaluated using Eqs. (2)–(3), is shown in Fig. 3b, which highlights the combined effect of cracking in the 90° and −45° plies. Fig. 3b also includes the predicted stress–strain response of Varna [23], Vyas and Pinho [34], and Daghia and Ladeveze [35] for the same laminate, which illustrates that our model, while comparable to other models, predicts relatively less nonlinearity due to damage progression. A close inspection of Fig. 3b reveals the cause of this discrepancy in the different model predictions — the stress–strain curves begin to deviate once the 45° ply cracks initiate. This is attributed to the variation in the predicted ±45° ply crack density evolution by the different models, as well as the corresponding stiffness degradation procedures employed [23,34,35].

In Fig. 4, we present the model results for a [0/+70$_4$/−70$_4$/0$_{1/2}$]$_s$ GFRP laminate, and comparisons are made with experimental data [9] as well as the model developed by Barbero and Cortes [36]. Clearly, our model shows a good agreement with the test data, where the initial stage of the crack density evolution curve is accurately captured, which was also demonstrated in Figs. 2 and 3 for other laminates. Some reported models are not capable of fully capturing the initial portion of the crack density curve. This is a very important feature of the current model and is attributed to an accurate representation of the stochastic
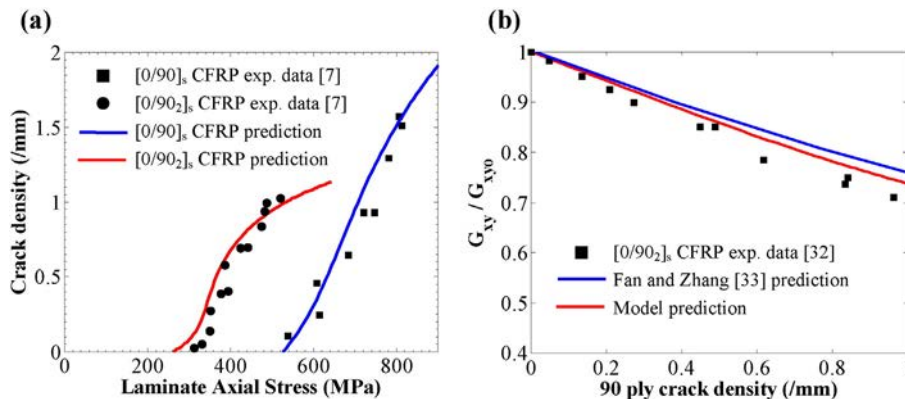

Fig. 2. Uniaxially loaded (a) [0/90]$_s$ and [0/90$_2$]$_s$ CFRP laminate predicted and experimental 90° ply crack density evolution, and (b) [0/90$_2$]$_s$ CFRP laminate predicted and experimental normalized shear stiffness degradation.
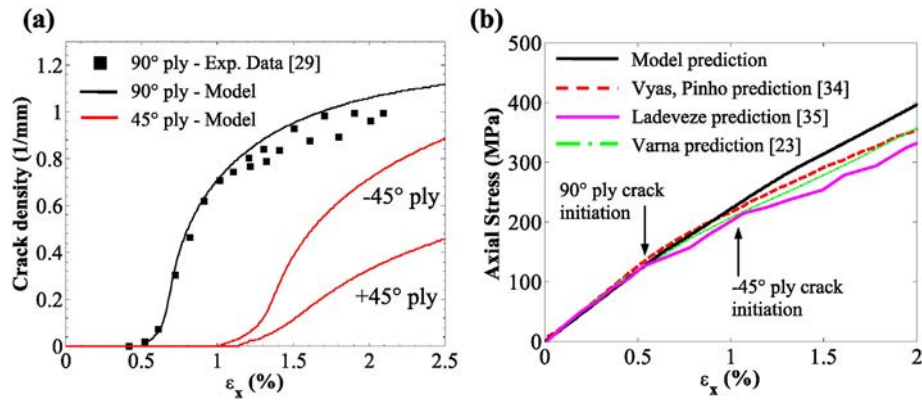
Fig. 3. Uniaxially loaded $[0/90/\mp 45]_s$ GFRP laminate predicted and experimental (a) ply crack density evolution, and (b) axial stress–strain response.

nature of G_{Ic}, as well as its dependency on the evolving crack density, as described in Ref. [25].

Next, damage evolution under equibiaxial tensile loading is considered for a $[\pm 45]_s$ angle-ply GFRP laminate. The crack density results are shown in Fig. 5a along with the predictions of Varna [23], which deviate slightly. This may be attributed to the different approaches used to account for intra-ply crack interactions (i.e., crack shielding). In our approach an inverse sigmoidal function fitted to the computationally obtained COD data is used to represent its variation with increasing crack density, while Ref. [23] utilized interaction functions for this purpose. Also, the crack initiation strain predicted by of our model corresponds to the reported value of 0.20% in Ref. [30], while the crack initiation strain predicted by Varna [23] has been over-estimated. The corresponding stress–strain response along with the available experimental stress–strain data [30] is shown in Fig. 5b. The stress–strain response is similar to that predicted by Varna and noticeably more accurate compared to the prediction of McCartney [13], however it deviates from the experimental data at strains greater than 1.2%. This is likely a result of neglecting the nonlinear shear response of the off-axis plies, which may be prevalent in this laminate. It should be noted that all model predictions under-predict stiffness degradation at higher strains as shown in Fig. 5b, which again may be due to an incorrect representation of the ply nonlinear shear response.

3.2. Damage evolution predictions under multi-axial loading

3.2.1. Cross-ply laminates

Fig. 6a shows crack density evolution plots for a $[0/90]_s$ CFRP cross-ply laminate subjected to biaxial loading, where the ply properties were taken from Ref. [7] (see Table 1). It is clear that a decrease in the biaxial loading ratio, σ_x/σ_y, slightly alters the crack evolution plots as is expected, with crack initiation occurring at lower applied axial loads. The effect of decreasing the biaxial loading ratio on the normalized laminate axial stiffness, E_x/E_{xo}, is shown in Fig. 6b, which reveals there is a slight increase in the stiffness degradation. Although the addition of an applied transverse strain does not directly increase σ_2^α in the 90° ply, the out-of-plane Poisson effect tends to increase the CODs in the cracked ply, thus causing slightly higher crack densities [24]. Evolution of the normalized laminate shear stiffness, G_{xy}/G_{xyo}, is shown in Fig. 6c, which demonstrates the effect of decreasing the biaxial loading ratio. The enhanced degradation of G_{xy} under biaxial conditions is due to the additional multiplication of 0° ply cracks, which do not influence the axial modulus.

3.2.2. Angle-ply laminates

Similar plots for a $[\pm 45]_s$ angle-ply GFRP laminate are presented in Fig. 7, with the ply properties taken from Ref. [29] (see Table 1). Clearly from Fig. 7a, a decrease in the biaxial loading ratio has a greater effect on the crack density evolution when compared to Fig. 6a, and the crack

initiation strain reduced from 1.25% to 0.3% for the uniaxial loading and equibiaxial cases, respectively. These results qualitatively compare to the predictions of Varna [23] for a similar angle-ply GFRP laminate. Under biaxial loading, off-axis plies will exhibit greater normal stresses, i.e., σ_2^α, and thus ply cracks initiate at lower applied loads, resulting in significant axial stiffness reduction as shown in Fig. 7b. Shear stiffness degradation plots are also shown in Fig. 7c. Due to the off-axis ply angle of 45°, the high laminate shear stiffness is less susceptible to degradation caused by ply cracking; however, the influence of a decreasing biaxial stress ratio is clear. The corresponding laminate axial stress–strain responses are illustrated in Fig. 7d, which demonstrates the effects of the altered crack density evolution and stiffness degradation on the laminate deformation behavior. Note that the effect of biaxial loading ratio on the stress–strain response is analogous to the predictions reported in Ref. [23] for a similar angle-ply laminate.

In order to investigate the effect of ply angle on the biaxial response of laminates, $[\pm 60]_s$ and $[\pm 75]_s$ angle-ply GFRP laminates were also analyzed. Crack density and axial stiffness degradation model results for these lay-ups are presented in Fig. 8, which demonstrates that as the off-axis ply angle, θ, increases the biaxial effects are reduced. It is intuitive that the contribution of the applied laminate transverse stress (σ_{yy}) on the transformed ply level stress acting normal to the fibers (i.e., σ_2^α) decreases with increasing off-axis ply angle. As a result, the applied transverse stress component does not contribute significantly to ply crack multiplication and axial stiffness degradation when $\theta > 45°$, rendering the laminate less susceptible to biaxial loading. Whereas when $\theta = 45°$, both the axial and transverse applied laminate stresses notably contribute to increasing σ_2^α, which describes the considerable change in crack density evolution for different biaxial stress ratios for this laminate. Also note that by comparing the uniaxial crack evolution plots in Figs. 7a and 8a and c, it is clear that the crack initiation strain
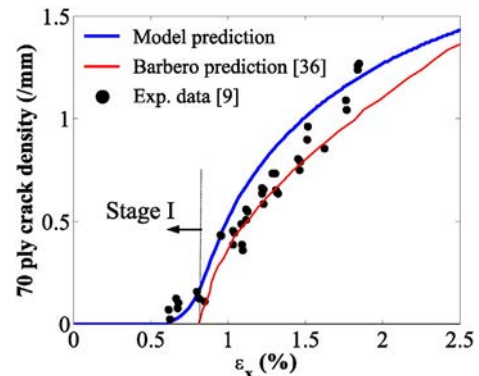

Fig. 4. Uniaxially loaded $[0/+70_4/-70_4/0_{1/2}]_s$ GFRP laminate predicted and experimental ply crack density evolution.
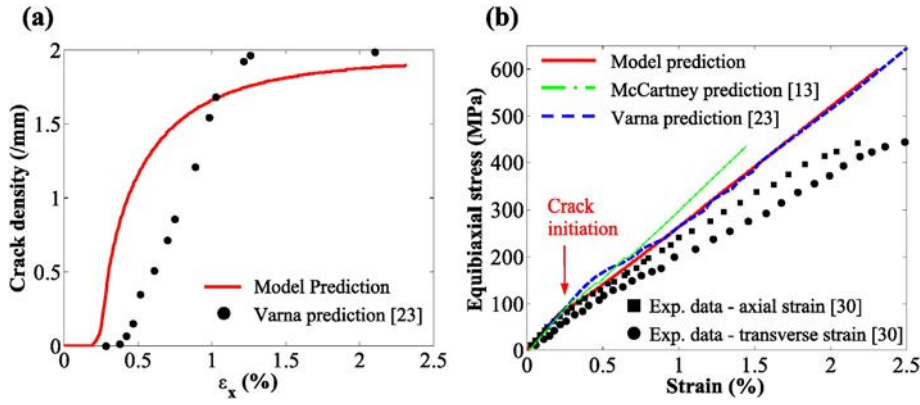
Fig. 5. Equibiaxially loaded $[\pm 45]_s$ GFRP laminate (a) predicted crack density evolution, and (b) predicted and experimental stress–strain response.

decreases as the off-axis ply angle increases, which has been experimentally observed [9].

3.2.3. [0/90/∓θ]ₛ GFRP laminates

Crack density evolution plots for a $[0/90/\mp 45]_s$ GFRP laminate subjected to biaxial loading conditions are shown in Fig. 9a and b, with ply properties taken from Ref. [29] (see Table 1). A decrease in biaxial loading ratio has a slight effect on 90° ply crack density and a more notable effect on 45° ply crack density, which is expected based on presented results for the $[0/90]_s$ and $[\pm 45]_s$ laminates. Specifically, crack initiation strains for 45° plies were 1.1% and 0.4% for uniaxial and equibiaxial cases, respectively. Crack density evolution plots in all plies for the equibiaxial loading case are shown in Fig. 9c, where all cracks initiate at an approximate strain of 0.4%. When compared to the uniaxial case for the same laminate (see Fig. 3a), this result is intuitive since local stresses (i.e., σ_2^α) driving crack multiplication are the same in each ply. Furthermore, since 90° and −45° plies are internal and constrained

on both sides, they exhibit the same crack density after saturation of approximately 1.25 cracks/mm. The external 0° ply and the thicker central +45° ply also exhibit similar crack density of 0.8 cracks/mm after saturation for the same equibiaxial loading case. The increased crack density for the internal plies is consistent with the trends reported in Ref. [37] for cross-ply laminates. The normalized shear modulus evolution for different biaxial loading ratios is shown in Fig. 9d, which demonstrates that the evolution of 0° ply cracks and the increase in 45° ply crack density causes a greater degradation in shear stiffness with decreasing biaxial loading ratio. The resulting laminate axial stress–strain responses are shown in Fig. 9e, where the effect of 45° ply cracks initiating at lower strains during biaxial loading is clearly demonstrated.

The model results for $[0/90/\mp 60]_s$ and $[0/90/\mp 75]_s$ GFRP laminates are presented in Fig. 10. By comparing $+\theta$ ply crack evolution for uniaxial loading in Figs. 9b and 10a and c, it is clear that increasing the off-axis ply angle causes cracks to initiate sooner and the crack saturation density to be higher. It is also evident in the same figures that the variation
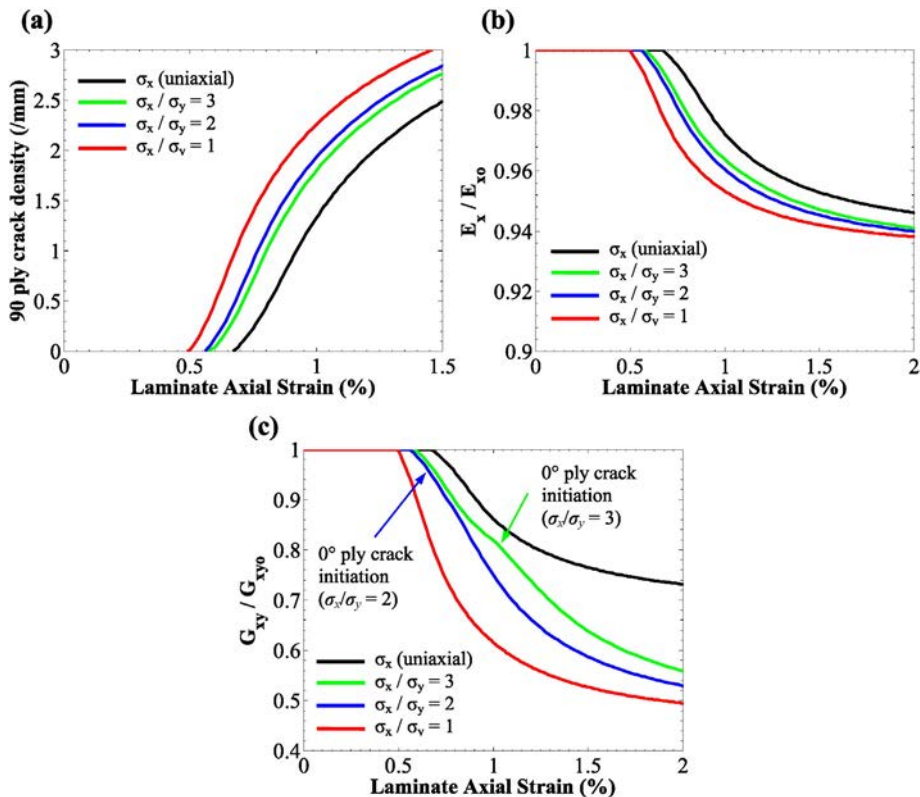

Fig. 6. Predicted results for a $[0/90]_s$ CFRP cross-ply laminate subjected to the indicated biaxial loading ratios (a) 90° ply crack density evolution, (b) normalized axial modulus evolution, and (c) normalized shear modulus evolution.
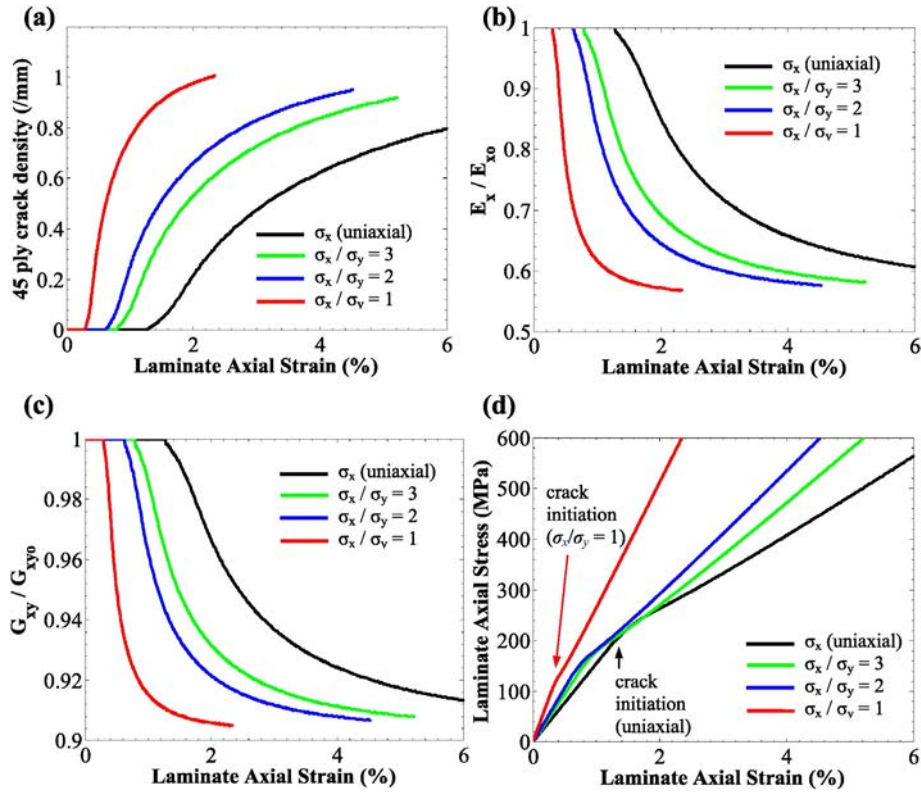
Fig. 7. Predicted results for a $[\pm 45]_s$ GFRP angle-ply laminate subjected to the indicated biaxial loading ratios (a) 45° ply crack density evolution, (b) normalized axial modulus evolution, (c) normalized shear modulus evolution, and (d) axial stress–strain response.

of $+\theta$ ply crack evolution with decreasing biaxial loading ratio decreases with increasing θ values. For example, the 45° crack initiation strain decreased from 1.1% to 0.4% for the uniaxial and equibiaxial

cases, whereas the 75° crack initiation strains decreased from 0.52% to 0.32% for the same loading cases. As the off-axis ply angle approaches 90°, the model is correctly predicting that the transverse loads have a
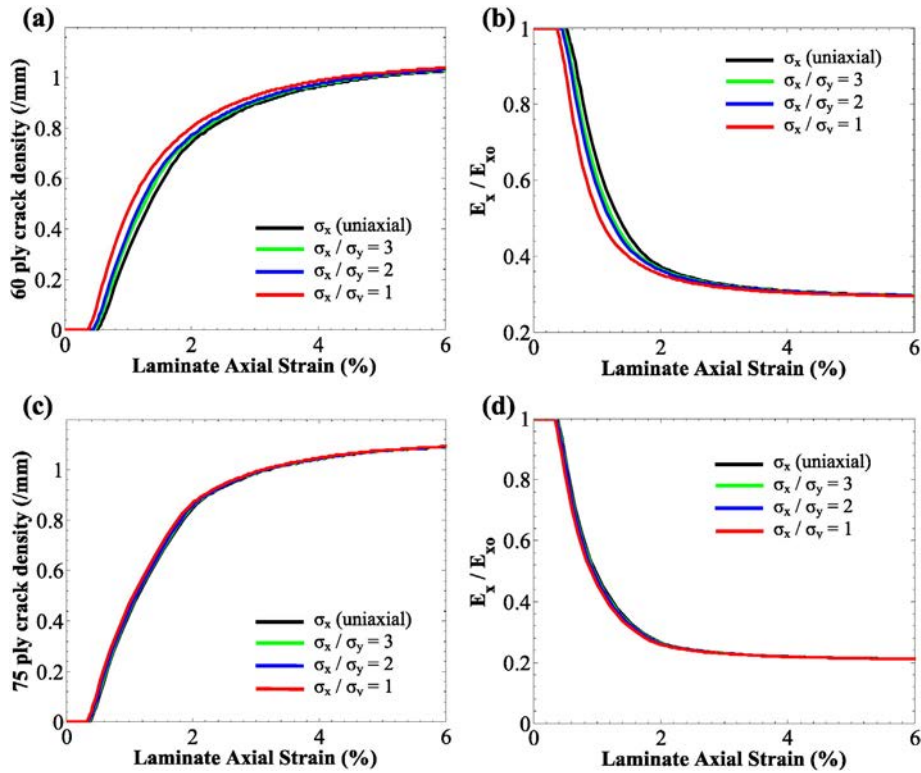

Fig. 8. Predicted results for GFRP angle-ply laminates subjected to the indicated biaxial loading ratios (a) $[\pm 60]_s$ ply crack density evolution, (b) $[\pm 60]_s$ normalized axial modulus evolution, (c) $[\pm 75]_s$ ply crack density evolution, and (d) $[\pm 75]_s$ normalized axial modulus evolution.

smaller effect on the crack density evolution in the off-axis plies. Furthermore, comparison of Figs. 9f and 10b, d clearly shows that as off-axis ply angle increases, the variation of normalized axial stiffness degradation with biaxial loading ratio decreases. Note that axial stiffness degradation magnitude is greater for higher off-axis ply angles as is expected.

3.3. Critical stiffness damage envelopes

As pointed out in the introduction, many practical composite structures have design functions that are stiffness critical. In such situations, it would be wise to develop critical damage envelopes corresponding to critical levels of stiffness properties, rather than strength characteristics. Here, we present critical stiffness damage envelopes for multiple laminate types predicted by extracting the data for damage evolution and stiffness changes as described in the preceding results. Since some industry practices preclude any design that allows existence of ply cracks, damage envelopes corresponding to initiation of ply cracks are also developed. Notably, the laminate crack initiation envelopes as depicted here correspond to the first cracking event in any ply of a given laminate, and represent the threshold for so-called first-ply failure events in the biaxial stress space. Critical stiffness damage envelopes, on the

other hand, represent the threshold for a particular magnitude of the laminate stiffness degradation for either the axial, E_x, or transverse, E_y, modulus. Only in-plane stiffness changes are considered in the present model. Out-of-plane deformations may need to include delamination modeling, which is a critical damage mechanism, and is thus excluded from consideration herein.

Damage envelopes for a $[0/90]_s$ cross-ply GFRP laminate are illustrated in Fig. 11a. The shape of crack initiation envelope results from the fact that 90° ply cracks are critical when $\sigma_x / \sigma_y > 1$, while the 0° ply cracks are critical when $\sigma_x / \sigma_y < 1$. Also, there seems to be a contention between the in-plane and out-of-plane Poisson effect. With respect to the laminate axial direction, the in-plane transverse load tends to delay the onset of 90° ply cracking since the axial strain decreases, while the corresponding added out-of-plane contraction tends to initiate cracking sooner as this increases the CODs [24]. The crack initiation curve in Fig. 11a depicts that these effects effectively cancel each other out since crack initiation occurs at approximately the same stress (e.g., see Fig. 6a), yielding the 'squared shape' envelope characteristic of cross-ply laminates [25]. It should be noted that since the inner 90° ply has an effective thickness that is twice that of the partially constrained 0° ply, they both have comparable crack initiation stresses under corresponding uniaxial loads, which further supports the shape
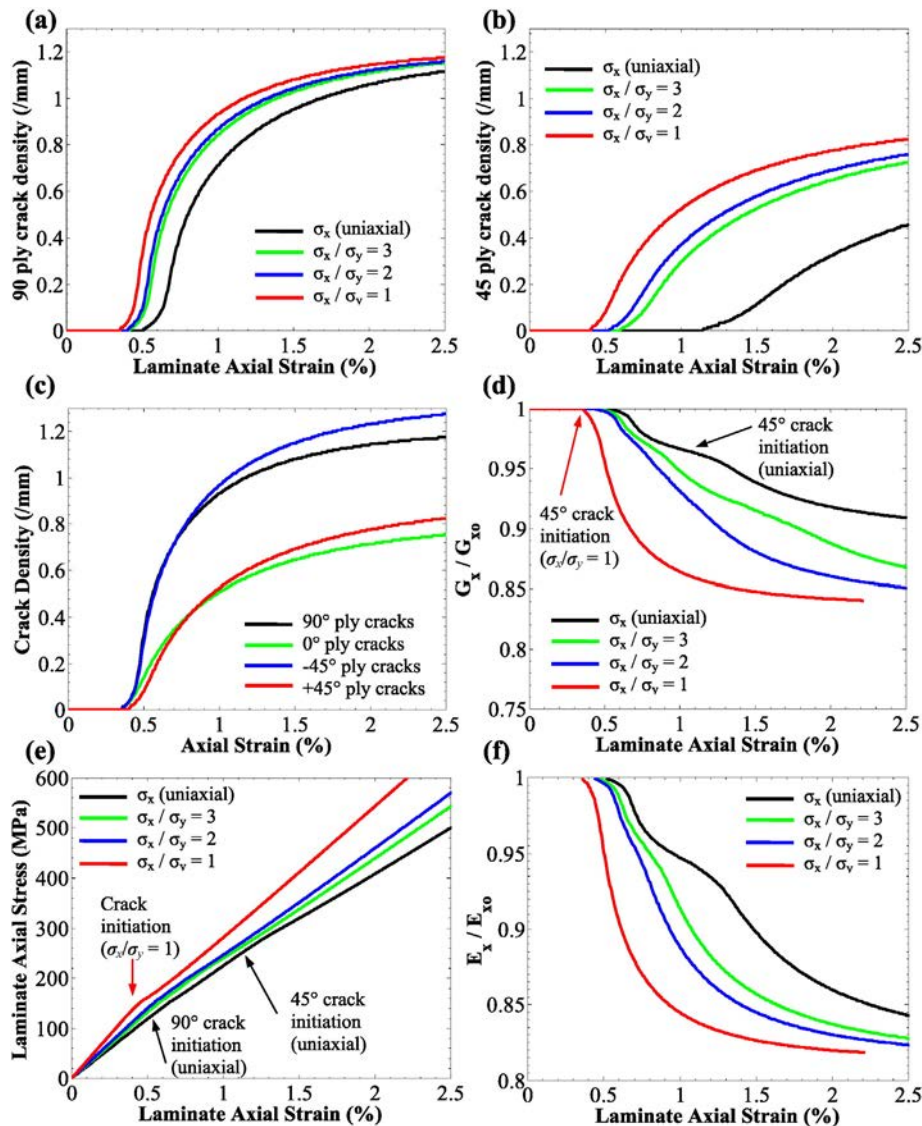

Fig. 9. Predicted results for a $[0/90/\mp45]_s$ GFRP quasi-isotropic laminate subjected to the indicated biaxial loading ratios (a) 90° ply crack density evolution, (b) +45° ply crack density evolution, (c) ply crack evolution for equibiaxial loading, (d) normalized shear modulus evolution, (e) axial stress–strain response, and (f) normalized axial stiffness degradation.

of the crack initiation curve in Fig. 11a. Regarding the critical stiffness damage envelopes shown in Fig. 11a, the variation of crack density in the adjacent plies (e.g., 0° ply cracks) during biaxial loading alters the crack evolution characteristics for the considered damage mode (e.g., 90° ply cracks), which is a result of the considered inter-ply crack interactions. Thus, the crack densities and stiffness properties at saturation vary for different σ_x / σ_y (e.g., see Fig. 6b), resulting in the distinct damage envelopes shown. It should be noted that the set of critical stiffness damage envelopes shown in Fig. 11a represent various critical regions of the biaxial stress space.

Fig. 11b, c and d show damage envelopes for $[\pm \theta]_s$ GFRP angle-ply laminates. For $[\pm 45]_s$ laminates, the longitudinal and axial stress components both drive cracking in the 45° plies during biaxial loading, where the increased local normal ply stress components cause ply cracks to initiate and saturate much sooner (see Fig. 7a). Thus, the shape of the crack initiation and damage envelopes are approximately linear as shown in Fig. 11b; the crack initiation results are analogous to the predictions reported in Refs. [20,35] for a similar $[\pm 45]_s$ laminate. When the off-axis ply angle increases to 60° or 75°, the transverse stress component has no effect on driving off-axis ply crack multiplication when $\sigma_x / \sigma_y > 1$ (see Fig. 8). As a result, the in-plane Poisson effect is notable as is shown in Fig. 11c and d by the slope of the envelopes. Also, since the off-axis ply angles are relatively high, cracks do not initiate when $\sigma_x / \sigma_y \ll 1$, and thus the critical stiffness magnitudes are not attained — see broken lines in Fig. 11c and d. In other words, under these loading conditions the laminates will not attain a critical stiffness prior to the onset of critical damage modes and final laminate failure.

Next, damage envelopes for a $[0/+55_4/-55_4/0_{1/2}]s$ GFRP laminate are presented in Fig. 12a. When $\sigma_x / \sigma_y > 1$, the axial and transverse stresses contribute to driving cracks in the off-axis plies, leading to the sloped portion of the crack initiation and damage envelopes as shown in Fig. 12a. For $\sigma_x / \sigma_y \ll 1$, crack driving stresses in the off-axis plies is minimal and the 0° plies become critical, resulting in a flat crack initiation curve since the in-plane Poisson effect is limited. For $\sigma_x / \sigma_y < 1$, both 0° ply cracks and off-axis ply cracks contribute to stiffness

degradation, and the resulting portion of the damage envelopes are sloped accordingly as shown in Fig. 12a. When the off-axis ply angle is increased to 70°, the crack initiation envelope shown in Fig. 12b is very similar to that of a cross-ply laminate (see Fig. 11a) since the transverse stress no longer drives cracking in the off-axis plies. Also, the corresponding damage envelopes in Fig. 12b are analogous to angle-ply laminates when $\theta = 60°$, and 75°.

Fig. 13a presents damage envelopes for a $[0/90/\mp 45]_s$ GFRP laminate. The crack initiation envelope shown is analogous to a cross-ply laminate (see Fig. 11a) since the 0° and 90° cracks are critical, and is consistent with the reported envelope in Ref. [38] for a similar quasi-isotropic laminate. For the damage envelope corresponding to 10% stiffness reduction in Fig. 13a, the shape is similar to the $[\pm 45]_s$ laminate (see Fig. 11b) due to the additional driving stresses on the off-axis plies. When the off-axis ply angle increases to 60° and 75°, the crack initiation envelopes shown in Figs. 13b and 13c are similar in shape to the $[0/90/\mp 45]_s$ laminate. Also for $\sigma_x / \sigma_y > 1$, the critical stiffness damage envelopes are similar to the $[0/90/\mp 45]_s$ laminate; however, when $\sigma_x / \sigma_y < 1$ the envelopes are distinct for the $[0/90/\mp 75]_s$ laminate. This is a result of the negligible effect of transverse stress on the off-axis ply cracks, which results in minor changes in stiffness degradation (see Fig. 10d). Thus, at these stress ratios critical stiffness is not attained prior to laminate failure.

It should be noted at this stage that the general shapes of the presented crack initiation and critical stiffness damage envelopes are notably different than conventional failure envelopes, which would be elliptical in shape for biaxial loading due to the in-plane Poisson's effect (for example see Ref. [16]). A failure envelope is included in Fig. 13a for the $[0/90/\mp 45]_s$ laminate, where failure is assumed to occur if the applied strain reaches a critical value of 2.5%. The accuracy of the failure criterion is not important here, nor do we condone using a failure criterion for stiffness critical designs, but it does suffice to demonstrate our point. As shown in Fig. 13a, the shape of the predicted failure envelope is elliptical as one would expect from a typical failure criterion. Therefore, this demonstrates that the distinct shapes of the damage envelopes
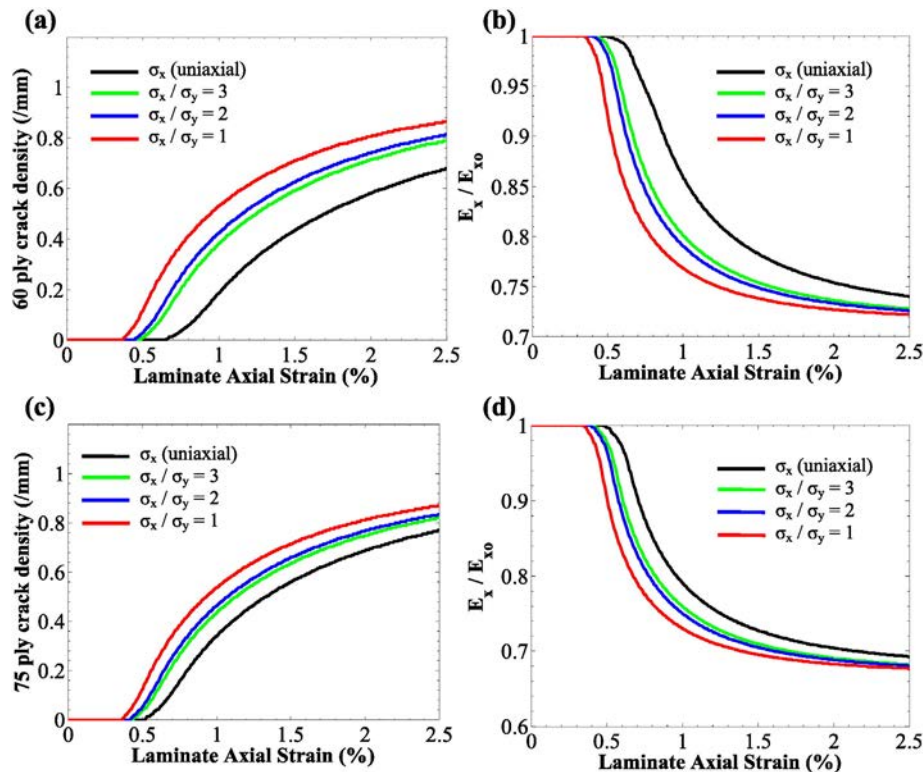

Fig. 10. Predicted results for GFRP laminates subjected to the indicated biaxial loading ratios: (a) $[0/90/\mp 60]_s$ + 60 ply crack density evolution, (b) $[0/90/\mp 60]_s$ normalized axial stiffness degradation, (c) $[0/90/\mp 75]_s$ + 75 ply crack density evolution, and (d) $[0/90/\mp 75]_s$ normalized axial stiffness degradation.
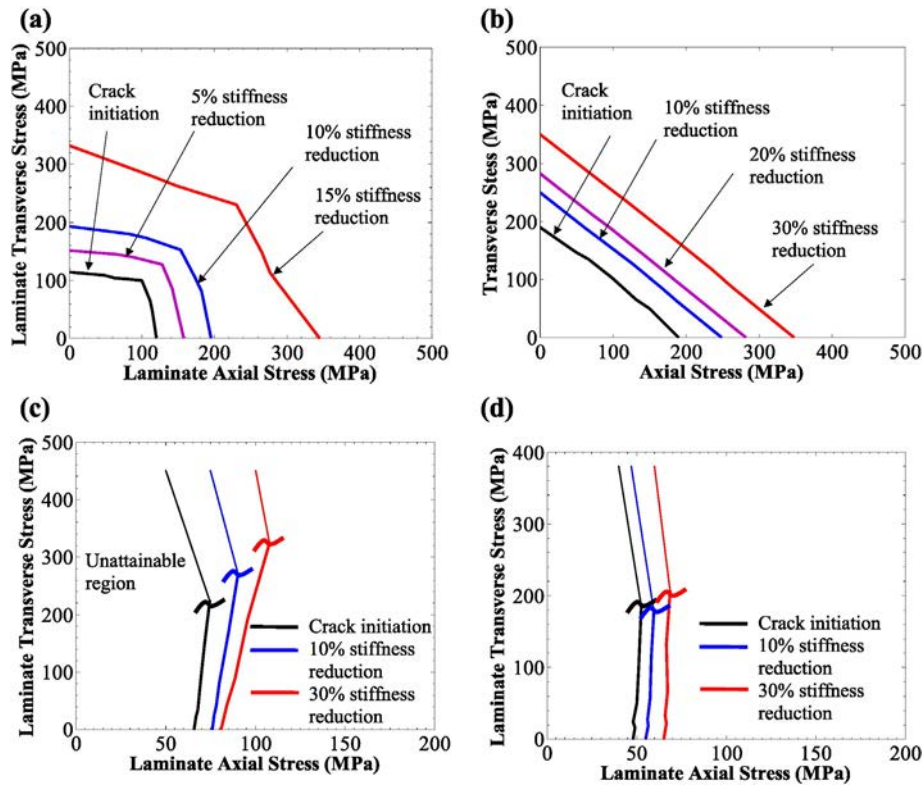
Fig. 11. Biaxial crack initiation envelopes and critical stiffness damage envelopes for (a) $[0/90]_s$ GFRP laminate, (b) $[\pm 45]_s$ GFRP laminate, (c) $[\pm 60]_s$ GFRP laminate, and (d) $[\pm 75]_s$ GFRP laminate.

in Figs. 11–13 result from complex ply crack evolution processes in the laminates studied.

3.4. Discussion

The ability of the developed model to predict damage evolution and stiffness degradation for various multidirectional laminates under multiaxial loading has clearly demonstrated its robustness. The proposed concept of using critical stiffness damage envelopes, in lieu of failure envelopes, as design criteria for stiffness critical structures is an important contribution of this work. However, there are some limitations with the model which are worth discussing at this stage. First, the model does not currently account for ply nonlinear shear stress–strain behavior. For angle-ply laminates this may contribute to their overall stress–strain response, which may improve the stress–strain predictions presented in Fig. 5b. Secondly, the model does not currently account for the effects of crack sliding displacements (CSD) for evaluation of the stiffness tensor

defined by Eq. (3). It is not clear at this stage whether or not the addition of CSDs will greatly influence the stiffness predictions for other laminate configurations not studied here. Furthermore, the scope of the prediction model is limited to predicting the evolution of sub-critical ply cracks, and the corresponding laminate stiffness degradation, prior to the onset of critical damage modes such as delamination and fiber fracture. This is suitable for predicting the durability of stiffness critical composite structures, and is in-line with the scope of this work. However, if the durability for a particular structural application must be predicted after the onset of critical damage modes, then these critical damage modes must be considered. This may involve the addition of delamination cracks in the computational micromechanical model. Finally, compressive damage modes are currently not considered by the model. It is clear that matrix cracks will still be the first sub-critical damage modes, but the evolution of these cracks under compressive loading must be investigated further.
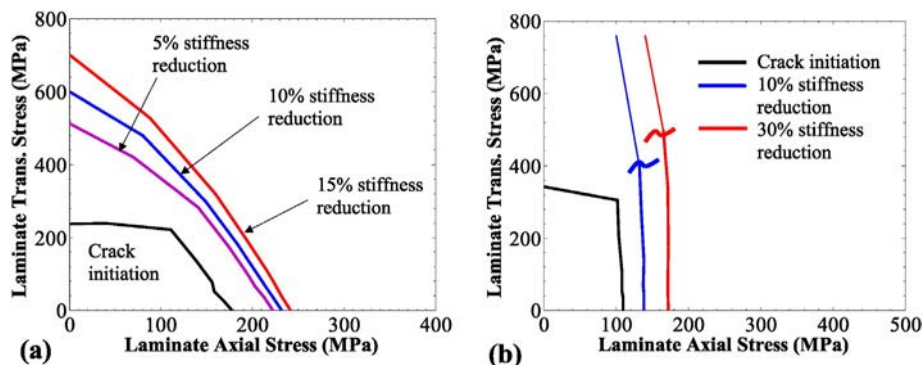

Fig. 12. Biaxial crack initiation envelopes and critical stiffness damage envelopes for (a) $[0/+55_4/-55_4/0_{1/2}]s$ GFRP laminate and (b) $[0/+70_4/-70_4/0_{1/2}]s$ GFRP laminate.
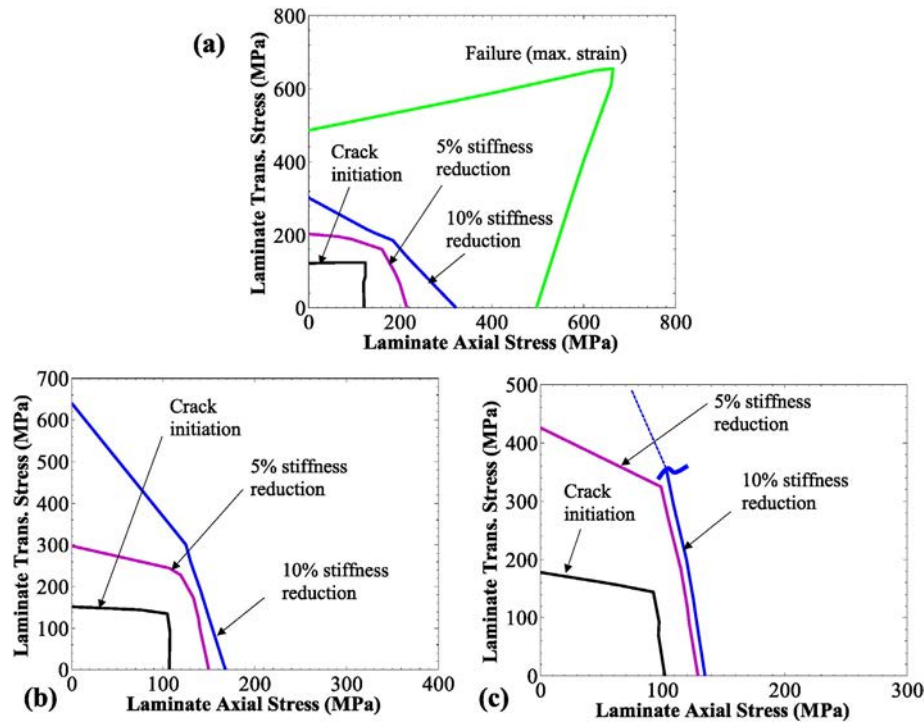
Fig. 13. Biaxial crack initiation envelopes and critical stiffness damage envelopes for (a) $[0/90/\mp45]_s$ GFRP laminate, (b) $[0/90/\mp60]_s$ GFRP laminate, and (c) $[0/90/\mp75]_s$ GFRP laminate.

4. Conclusions

This paper presented the predictions of a developed multiscale progressive damage model, where the behavior of various multidirectional laminates subjected to multiaxial loading was studied. The model coherently combined computational micromechanics with continuum damage mechanics in a synergistic damage mechanics framework to evaluate the corresponding laminate stiffness degradation, whereby the computational micromechanical model inherently accounted for crack interactions and ply constraining effects. This is seen as a clear advantage over existing models since it eliminated the need for costly empirical calibration. Furthermore, an energy-based approach was utilized to predict the evolution of sub-critical ply cracks under multiaxial loading. This model accounted for the variation of critical strain energy release rate, G_{Ic}, for ply cracks in the different laminate plies. This is an advantage over existing models that assume constant G_{Ic} for all plies, and is important requirement for multiaxial loading conditions.

The model predictions for several GFRP and CFRP cross-ply and multidirectional laminates correlated well with available uniaxial and biaxial experimental data, including crack evolution, stiffness degradation and stress–strain response data, providing validation for its accuracy. Predictions for several multidirectional laminates with different stacking sequences, subjected to various biaxial loading conditions, demonstrated the model's capabilities and its robustness. In addition, the new concept of critical stiffness damage envelopes was presented. The predicted damage envelopes were proposed as design criteria for stiffness critical composite structures, where failure is not defined in the traditional sense as a loss in load bearing capacity, but rather when a critical stiffness or a maximum deflection of the structure is attained. It should also be noted that the developed model is suitable for implementation into commercial finite element packages in order to analyze damage evolution in composite structures, and can also be extended to account for damage evolution due to cyclic loading (i.e., damage tolerance analysis). This will ultimately provide a comprehensive means to predict the structural integrity and durability of stiffness critical composite structures, which may include helicopter rotors, robotic linkages, wind turbines, and pressure vessels.

References

[1] J.E. Masters, K.L. Reifsnider, An investigation of cumulative damage development in quasi-isotropic graphite/epoxy laminates, in: K.L. Reifsnider (Ed.), Damage in Composite Materials — ASTM STP 775 1982, pp. 40–62 (Philadelphia).
[2] T.C. Moon, H.Y. Kim, W. Hwang, Natural-frequency reduction model for matrix-dominated fatigue damage of composite laminates, Compos. Struct. 62 (2003) 19–26.
[3] R. Talreja, Assessment of the fundamentals of failure theories for composite materials, Compos. Sci. Technol. 105 (2014) 190–201.
[4] P.D. Soden, A.S. Kaddour, M.J. Hinton, Recommendations for designers and researchers resulting from the world-wide failure exercise, Compos. Sci. Technol. 64 (2004) 589–604.
[5] Z. Hashin, Analysis of cracked laminates: a variational approach, Mech. Mater. 4 (1985) 121–136.
[6] R. Talreja, Transverse cracking and stiffness reduction in composite laminates, J. Compos. Mater. 19 (1985) 355–375.
[7] J. Zhang, J. Fan, C. Soutis, Analysis of multiple matrix cracking in $[\pm\theta_m/90_n]_s$ composite laminates — part 2: development of transverse ply cracks, Composites 23 (1992) 299–304.
[8] R. Joffe, A. Krasnikovs, J. Varna, COD-based simulation of transverse cracking and stiffness reduction in $[S/90_n]_s$ laminates, Compos. Sci. Technol. 61 (2001) 637–656.
[9] J. Varna, R. Joffe, V.N. Akshantala, R. Talreja, Damage in composite laminates with off-axis plies, Compos. Sci. Technol. 59 (1999) 2139–2147.
[10] C.V. Singh, R. Talreja, A synergistic damage mechanics approach for composite laminates with matrix cracks in multiple orientations, Mech. Mater. 41 (2009) 954–968.
[11] C.V. Singh, R. Talreja, Evolution of ply cracks in multidirectional composite laminates, Int. J. Solids Struct. 47 (2010) 1338–1349.
[12] C.V. Singh, R. Talreja, A synergistic damage mechanics approach to mechanical response of composite laminates with ply cracks, J. Compos. Mater. 47 (2013) 2475–2501.
[13] L.N. McCartney, Predicting transverse crack formation in cross-ply laminates, Compos. Sci. Technol. 58 (1998) 1069–1081.
[14] P. Xu, J.Y. Zheng, P.F. Liu, Finite element analysis of burst pressure of composite hydrogen storage vessels, Mater. Des. 30 (2009) 2295–2301.
[15] D. Zhang, J. Ye, D. Lam, Ply cracking and stiffness degradation in cross-ply laminates under biaxial extension, bending and thermal loading, Compos. Struct. 75 (2006) 121–131.

[16] J.S. Welsh, J.S. Mayes, A.C. Biskner, 2-D biaxial testing and failure predictions of IM7/977-2 carbon/epoxy quasi-isotropic laminates, Compos. Struct. 75 (2006) 60–66.

[17] P.F. Liu, J.Y. Zheng, Recent developments on damage modeling and finite element analysis for composite laminates: a review, Mater. Des. 31 (2010) 3825–3834.

[18] J.A. Mayugo, P.P. Camanho, P. Maimi, C.G. Davila, Analytical modelling of transverse matrix cracking of $\{\pm\theta/90_n\}_s$ composite laminates under multiaxial loading, Mech. Adv. Mater. Struct. 17 (2010) 237–245.

[19] E.J. Barbero, G. Sgambitterra, A. Adumitroaie, X. Martinez, A discrete constitutive model for transverse and shear damage of symmetric laminates with arbitrary stacking sequence, Compos. Struct. 93 (2011) 1021–1030.

[20] F. Laurin, N. Carrere, C. Huchette, J.F. Maire, A multiscale hybrid approach for damage and final failure predictions of composite structures, J. Compos. Mater. 47 (2013) 2713–2747.

[21] M. Kashtalyan, C. Soutis, Predicting residual stiffness of cracked composite laminates subjected to multi-axial inplane loading, J. Compos. Mater. 47 (2013) 2513–2524.

[22] M.R. Satapathy, B.G. Vinayak, K. Jayaprakash, N.K. Naik, Fatigue behaviour of laminated composites with a circular hole under in-plane multiaxial loading, Mater. Des. 51 (2013) 347–356.

[23] J. Varna, Modelling mechanical performance of damaged laminates, J. Compos. Mater. 47 (2013) 2443–2474.

[24] J. Montesano, C.V. Singh, A synergistic damage mechanics based multiscale model for composite laminates subjected to multiaxial strains, Mech. Mater. 83 (2015) 72–89.

[25] J. Montesano, C.V. Singh, Predicting evolution of ply cracks in composite laminates subjected to biaxial loading, Compos. Part B 75 (2015) 264–273.

[26] R. Talreja, Damage characterization by internal variables, in: R. Talreja (Ed.), Damage Mechanics of Composite Materials, Elsevier, Amsterdam 1994, pp. 53–78.

[27] P.P. Camanho, C.G. Davila, S.T. Pinho, L. Iannucci, P. Robinson, Prediction of in situ strengths and matrix cracking in composites under transverse tension and in-plane shear, Compos. Part A 37 (2006) 165–176.

[28] J.M. Berthelot, J.F. LeCorre, Statistical analysis of the progression of transverse cracking and delamination in cross-ply laminates, Compos. Sci. Technol. 60 (2000) 2659–2669.

[29] J. Tong, F.J. Guild, S.L. Ogin, P.A. Smith, On matrix crack growth in quasi-isotropic laminates — I. Experimental investigation, Compos. Sci. Technol. 57 (1997) 1527–1535.

[30] P.D. Soden, M.J. Hinton, A.S. Kaddour, Biaxial test results for strength and deformation of a range of e-glass and carbon fiber reinforced composite laminates: failure exercise benchmark data, Compos. Sci. Technol. 62 (2002) 1489–1514.

[31] P.D. Soden, M.J. Hinton, A.S. Kaddour, Lamina properties, lay-up configurations and loading conditions for a range of fibre-reinforced composite laminates, Compos. Sci. Technol. 58 (1998) 1011–1022.

[32] C.L. Tsai, I.M. Daniel, The behaviour of cracked cross-ply composite laminates under shear loading, Int. J. Solids Struct. 29 (1992) 3251–3267.

[33] J. Fan, J. Zhang, In-situ damage evolution and micro/macro transition for laminated composites, Compos. Sci. Technol. 47 (1993) 107–118.

[34] G.M. Vyas, S.T. Pinho, Computational implementation of a novel constitutive model for multidirectional composites, Commun. Math. Sci. 51 (2012) 217–224.

[35] F. Daghia, P. Ladeveze, Identification and validation of an enhanced mesomodel for laminated composites within the WWFE-III, J. Compos. Mater. 47 (2013) 2675–2693.

[36] E.J. Barbero, D.H. Cortes, A mechanistic model for transverse damage initiation, evolution and, stiffness reduction in laminated composites, Compos. Part B 41 (2010) 124–132.

[37] J.A. Nairn, S. Hu, The formation and effect of outer-ply microcracks in cross-ply laminates: a variational approach, Eng. Fract. Mech. 41 (1992) 203–221.

[38] C.T. Sun, J. Tao, Prediction of failure envelopes and stress/strain behaviour of composite laminates, Compos. Sci. Technol. 58 (1998) 1125–1136.